Integration of Water Management into the Energy Management Strategy for a Fuel Cell Vehicle

Mohammadreza Moghadari, Mohsen Kandidayeni, *Member, IEEE*, Ashkan Makhsoos, Loïc Boulon, *Senior Member, IEEE*, and Hicham Chaoui, *Senior Member, IEEE*

***Abstract*— Unlike other studies that focus solely on determining the optimal power distribution for a fuel cell hybrid electric vehicle (FC-HEV), this paper aims to integrate water management into the energy management strategy (EMS) by designing an adaptive efficient purge strategy. This study investigates the impact of integrated water management into the EMS (IWM-EMS) on the performance and operating cost of FC-HEV. The IWM-EMS consists of two levels: the first level is the EMS, which determines the optimal power, and the second level is the proposed purge strategy. The proposed IWM-EMS in this study is the adaptive IWM-EMS (AIWM-EMS), which utilizes an adaptive efficient purge strategy that can adjust based on the FC reference current. Another IWM-EMS is the non-adaptive IWM-EMS (NAIWM-EMS), which utilizes a constant purge strategy suggested by the FC manufacturer for all current levels. The results show that the FC-HEV under the AIWM-EMS consumes 4.09% less hydrogen than the NAIWM-EMS and reduces total operating cost by up to 5.21%. In addition, 78.36% of the FCs' operating time is spent in the high-efficiency zone.**

***Index Terms*— Energy management strategy, proton exchange membrane fuel cell, purge strategy, voltage stability, water management.**

I. Introduction

A. Literature Review

ALIGNED with green transportation policies, fuel cell hybrid electric vehicles (FC-HEVs) have gained significant attention in the field of vehicle electrification, with widespread development in many countries around the world [1]. Proton exchange membrane fuel cells (PEMFCs) are employed as the primary power source in FC-HEVs due to their distinct characteristics, including high efficiency, low operating temperatures, rapid start-up times, and nearly zero emissions [2]. However, due to the slow dynamic response of the FC, a secondary power source, such as a battery or supercapacitor (SC), is utilized in FC-HEVs [3]. In FC-HEVs, due to the existence of multiple power sources with distinct characteristics, an energy management strategy (EMS) is needed to effectively manage power distribution [4], [5]. According to the literature, EMSs typically fall into three main categories: rule-based (RB), optimization-based (OB), and learning-based (LB) [6]. In the literature, various EMSs and their combinations are explored. The study in [7] proposes a frequency-decoupling EMS using fuzzy control for a FC-HEV. The proposed strategy enhances power performance, reduces FC degradation, and improves fuel economy by 7.94%. In [8], the authors propose an adaptive state machine as a RB-EMS for a multi-stack FC-HEV. The proposed EMS improves fuel efficiency and reduces FC degradation. In [9], a nonlinear model predictive control (NMPC)-based EMS is proposed for FC-HEVs. The results show that the proposed EMS enhances fuel efficiency, minimizes hydrogen consumption, and reduces FC degradation. The study in [10] proposes an online efficiency-optimized EMS for a FC-HEV. The results show an efficiency increase to 53% and a reduction in computational burdens. In [11], a hierarchical EMS for a FC-HEV using deep reinforcement learning (DRL) is developed. The proposed EMS improves FC lifespan and enhances fuel economy by 16.8%. The paper in [12] presents a three-level EMS for FC-HEV, utilizing a dual-reward Q-learning algorithm. This strategy improves energy efficiency by 8% and reduces FC degradation.

B. Impact of Water Management on Voltage Stability

In real-time applications like vehicles, the performance, durability, and reliability of PEMFC systems are challenging and largely depend on effective water management [13]. PEMFC performance highly depends on the membrane's hydration level, and an imbalance in hydration can reduce proton conductivity and lower overall performance. Water transport in a PEMFC involves three main processes that influence membrane's water balance and overall performance. The first is water generation on the cathode side during the oxygen reduction reaction, which increases with current. The second process is back diffusion, where water moves from the cathode to the anode due to concentration differences. The third is electro-osmotic drag, which pulls water molecules, along with protons through the membrane toward the cathode [14], [15]. Water flooding and membrane drying out are two common faults in PEMFC associated with water management malfunctions [16]. An increase in the membrane's hydration level can lead to flooding, which restricts the access of reactant gases and reduces PEMFC performance. Back diffusion is a key contributor to this issue. On the other hand, a decrease in membrane hydration causes drying out, leading to higher membrane resistance and reduced proton conductivity. Electro-osmotic drag is a primary factor contributing to drying out [16], [17]. Flooding and drying out can reduce the PEMFC output voltage and power in the short term. If not resolved promptly, they can result in long-term effects, eventually leading to PEMFC failure [17].

One of the feasible and economical solutions to improve water management in PEMFCs is the use of a purge valve. This approach is particularly common in dead-end anode (DEA) PEMFCs [13]. Using the purge valve is an effective method for promptly removing accumulated water and helping the PEMFC quickly return to a normal and healthy condition. Determining an appropriate purge strategy is crucial for effective water management. Some studies focus on analyzing the impact of different purge strategies on the water content inside the PEMFC [18]–[21]. However, this approach relies on a precise model to estimate the water content, which is challenging due to the complexity and multi-physics nature of PEMFCs. Consequently, it may not effectively enhance water

management. One important aspect of designing a suitable purge strategy is its effectiveness in real-time applications. Using a precise water content model requires a three-dimensional approach, which is complex and increases the computational burden. This can compromise the real-time applicability of purge strategy design. Moreover, an accurate dynamic model of water content depends on several parameters, which remains a limitation in current studies.

Voltage, as the output of a FC system, is a vital parameter with a significant impact on FC performance. It acts as an indicator, where any drop signals a malfunction in the FC. On the other hand, in real-world applications such as FC-HEVs, quickly detecting water management faults and taking appropriate action to resolve them and restore PEMFC performance is highly important. PEMFC voltage is a dependable indicator of performance and can be measured easily without the need for complex sensors. Therefore, to avoid the complexity and inaccuracies of water content models, voltage monitoring (VM) is a reliable and widely used method for improving water management and detecting PEMFC malfunctions in real-world applications [16]. As unstable voltage is a consequence of water management faults, maintaining voltage stability through an appropriate purge strategy ensures effective water management in the PEMFC. In this regard, many studies on purge strategies focus on voltage stability as the output of the PEMFC system to improve water management. These types of studies focus on designing suitable purge strategies to achieve effective water management by analyzing voltage stability [22]–[24]. In these studies, voltage is considered stable if the drop during the purge interval is less than 100 mV [22], [23], [25]. Fig. 1 shows the effect of the purge strategy on water management and voltage stability at 42 A in an H-500 DEA-PEMFC with a 20 s purge interval. The dashed red line represents the desired voltage, while the blue line displays experimental data. At 42 A, a 100 ms purge duration fails to remove accumulated water, resulting in flooding and a 917.5 mV voltage drop, which exceeds the stability limit. A 600 ms duration guarantees proper water management and reduces the voltage drop to 72.5 mV.

Despite the effectiveness of the purge method in PEMFCs, an important issue with this system is the wasted hydrogen during the purge. Since hydrogen is an expensive fuel, considering wasted hydrogen when designing a suitable purge strategy is essential, as it significantly impacts system efficiency and PEMFC operating cost [13], [26]. However, there are few studies focused on designing an efficient purge strategy that maintains voltage stability while minimizing hydrogen consumption [27]–[29].

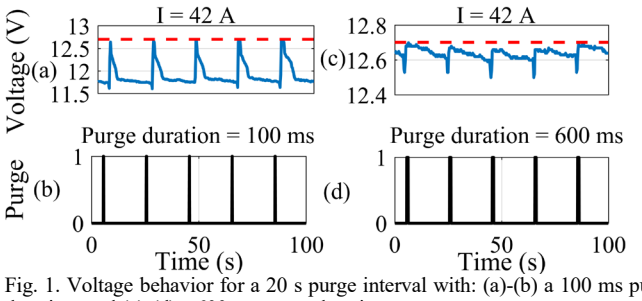

Fig. 1. Voltage behavior for a 20 s purge interval with: (a)-(b) a 100 ms purge duration; and (c)-(d) a 600 ms purge duration.

C. Contributions

PEMFC operating current plays a key role in water management. An increase in PEMFC current intensifies water flooding [30]. Although in some commercial PEMFC systems purge parameters are tuned with current levels, the literature review illustrates that academic and laboratory-scaled studies on purge strategies in PEMFCs focus only on designing a constant, non-adaptive purge strategy for all current levels. Due to current changes in real-world applications and the sensitivity of PEMFC performance to the output current, designing an adaptive purge strategy that can adjust to different current levels can reduce the risk of water management faults and improve PEMFC voltage stability. However, despite the critical role of current in PEMFC performance and voltage behavior, considering current variations when designing a purge strategy is rarely addressed. As a result, since in real-world applications PEMFC operating conditions are always dynamically changing, the first contribution of this study is to design a purge strategy that can adapt to various dynamic conditions. In this regard, an adaptive efficient purge strategy is proposed, which adjusts based on the PEMFC operating current.

In vehicular applications, water management faults are the most common issues and cause unstable or decreased voltage. In real-world applications like FC-HEVs, voltage stability is crucial to ensure the requested power is supplied. As a result, considering water management and its effect on voltage stability is crucial in real-world applications. Despite its critical importance in real-world applications, the integration of water management into an EMS has not been addressed. In this regard, the second contribution of this paper is the design of an integrated water management into the EMS (IWM-EMS) utilizing an adaptive efficient purge strategy. The proposed purge strategy is implemented in a hardware-in-the-loop (HIL) setup to evaluate its effectiveness.

II. Design of a Purge Strategy Through Experimental Analysis

A. Experimental Setup

This study utilizes an air-cooled open-cathode DEA-PEMFC manufactured by Horizon Fuel Cell Technologies for experiments at the Hydrogen Research Institute's test center, located at the Université du Québec à Trois-Rivières (UQTR) [31]. Table I shows the technical characteristics of the H-500 DEA-PEMFC. To develop a suitable purge strategy that avoids water management faults and ensures stable PEMFC voltage, this study conducts extensive tests using seven purge intervals (8–20 s) and eight purge durations (100–1000 ms) across current levels ranging from 1 to 42 A. Table II illustrates the proposed experimental plan. The 8 s interval is used to assess water management and voltage behavior below the 10 s purge interval recommended by manufacturers, while the 20 s interval is used to examine the effects of a longer purge interval. Purge durations are selected based on the chosen purge interval range.

TABLE I
Technical Characteristics of the H-500 DEA-PEMFC

Number of cells	24
Rated Power	500W
Voltage range	12-23 V
Maximum current	42 A
Operating temperature	0 - 65 °C
Cooling system	Cooling fan (ambient air)

TABLE II
EXPERIMENTAL PLAN

Purge combinations		Current levels
Purge interval (s)	Purge duration (ms)	1 A, 2 A, 3A, …, 41 A, 42 A
8, 10, 12, 14, 16, 18, 20	100,200, 300, 400, 500, 600 700 1000	

While most studies and PEMFC data sheets recommend a minimum duration above 100 ms, this study uses 100 ms to investigate its effect on water management and voltage stability. The 1000 ms duration is defined as the upper limit, considered a safe and conservative choice. Experimental results confirm that combining this maximum duration with various intervals ensures effective water removal and maintains voltage stability.

In each test, the H-500 DEA-PEMFC runs for 10 minutes to reach a steady state. The data from the last 100 s is collected for analysis. In the developed PEMFC test center, the ambient temperature and humidity are 21 °C and 46%, respectively, and a control system maintains these environmental conditions during the experiments to improve the quality of the experimental results. It should be noted that the PEMFC fan duty cycle is 80% to ensure the stack temperature stays within a safe range during the purge strategy tests.

B. Voltage Behavior Analysis

In this section, the voltage behavior is analyzed for four different currents (10 A, 20 A, 30 A, and 42 A), representing low, medium, and high current levels. In the voltage behavior analysis, 100 mV is selected as the threshold for unstable voltage, as exceeding this value can lead to water management faults.

1) Voltage Analysis of the Manufacturer's Suggested Non-Adaptive Purge Strategy: The purge strategy suggested by the H-500 manufacturer consists of a purge interval of 10 s and a duration of 100 ms. Fig. 2(a)-(d) shows the voltage behavior, and Fig. 2(e) displays the status of the purge valve. As shown in Fig. 2(a)-(b), the average voltage drops during the purge intervals are 25 mV at 10 A and 21.11 mV at 20 A, indicating that the PEMFC is operating safely without water management faults. According to Fig. 2(c)-(d), the average voltage drops are 250 mV for 30 A and 553 mV for 42 A, exceeding the 100 mV threshold. Fig. 2(c)-(d) demonstrates that the 10 s purge interval and 100 ms purge duration recommended by the manufacturer are unsuitable for high currents and result in flooding and voltage drop. Therefore, the results highlight the importance of an appropriate purge strategy to improve water management and maintain voltage stability, especially at high currents.

2) The Impact of Purge Interval and Duration on Voltage Stability: This section focuses on analyzing how changes in the purge interval and duration impact water management and voltage behavior. For this analysis, purge intervals of 8 s, 14 s, and 20 s are selected as samples to demonstrate PEMFC voltage behavior. Fig. 3(a)-(d) illustrates voltage behavior with a purge interval of 8 s and a 100 ms purge duration. The average PEMFC voltage drops during the purge interval are provided in Table III. According to Fig. 3(a)-(b) and Table III, for an 8 s purge interval, the 100 ms purge duration is suitable for 10 A and 20 A, as the average voltage drop remains below 100 mV. However, it is not suitable for high currents like 30 A and 42 A. According to Fig. 3(f)-(i) and Table III, for the 8 s purge interval the 200 ms purge duration is suitable since the average voltage drop for all currents remains below 100 mV.

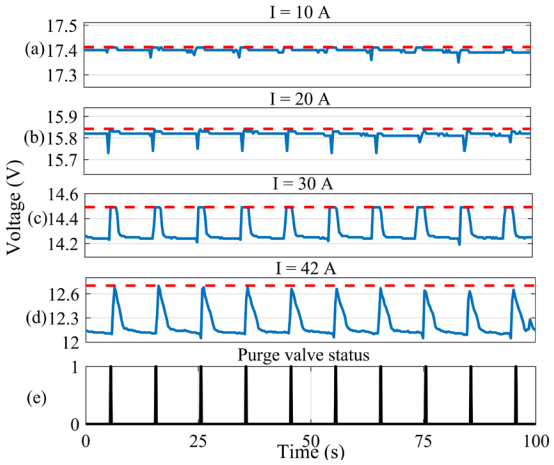

Fig. 2. Voltage behavior for a 10 s purge interval and 100 ms purge duration at different currents: a) 10 A; b) 20 A; c) 30 A; d) 42 A; e) Purge valve status.

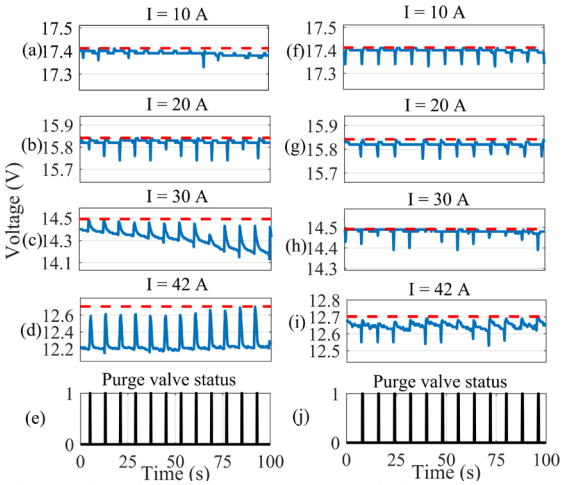

Fig. 3. Voltage behavior for a purge interval of 8 s and a 100 ms duration: (a)-(e), and for a purge interval of 8 s with a 200 ms duration: (f)-(j).

TABLE III
AVERAGE VOLTAGE DROPS FOR A PURGE INTERVAL OF 8 S WITH DIFFERENT PURGE DURATIONS

Purge interval (s) - Purge duration (ms)					
8 - 100	Current (A)	10	20	30	42
	Voltage drop (mV)	15	19.10	162.5	420
8 - 200	Voltage drop (mV)	13.33	17	15.83	51.82

Fig. 4(a)-(d) shows the PEMFC voltage behavior with a purge interval of 14 s and a purge duration of 100 ms. According to Fig. 4(a)-(d) and Table IV, a 100 ms purge duration for current levels of 30 A and 42 A is insufficient to recover PEMFC performance. Fig. 4(f)-(i) indicates the voltage behavior with the 14 s purge interval and the 200 ms purge duration. The results of Fig. 4(f)-(i) and Table IV show that the 200 ms purge duration is not sufficient for a current of 42 A to remove the excess water and stabilize the voltage. According to Table IV, for a 14 s purge interval, a purge duration of 400 ms is suitable for an effective water management.

In this study, the maximum purge interval is 20 s. By analyzing different purge durations, Table V indicates that a

purge duration of 600 ms is suitable for a 20 s purge interval, as the voltage drop for all currents remains below 100 mV.

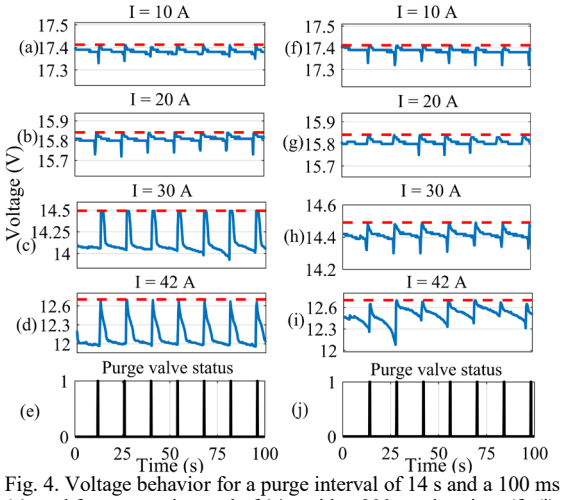

Fig. 4. Voltage behavior for a purge interval of 14 s and a 100 ms duration: (a)-(e), and for a purge interval of 14 s with a 200 ms duration: (f)-(j).

TABLE IV
AVERAGE VOLTAGE DROPS FOR A PURGE INTERVAL OF 14 S WITH DIFFERENT PURGE DURATIONS

Purge interval (s) - Purge duration (ms)					
14 - 100	Current (A)	10	20	30	42
	Voltage drop (mV)	28.33	38.33	463.67	698.19
14 - 200	Voltage drop (mV)	23.33	36.67	83.33	220
14 - 300	Voltage drop (mV)	18.25	30	73.26	136.67
14 - 400	Voltage drop (mV)	13	27.55	66.67	93.13

TABLE V
AVERAGE VOLTAGE DROPS FOR A PURGE INTERVAL OF 20 S WITH DIFFERENT PURGE DURATIONS

Purge interval (s) - Purge duration (ms)					
20 - 100	Current (A)	10	20	30	42
	Voltage drop (mV)	65	132.50	732.50	917.50
20 - 200	Voltage drop (mV)	45	80	475	525.67
20 - 300	Voltage drop (mV)	35.33	73.33	235	242.50
20 - 400	Voltage drop (mV)	25.33	50	102.50	195.33
20 - 500	Voltage drop (mV)	23.57	35	82	113.76
20 - 600	Voltage drop (mV)	20	27.50	75	72.50

Table VI shows the appropriate purge durations for all purge intervals used in this study. Based on the analysis of experimental results, for a constant purge interval, increasing the purge duration mitigates water management faults. Conversely, for a constant purge duration, increasing the purge interval leads to increased water management faults and unstable voltage.

C. Impact of the Purge Strategy on Hydrogen Consumption

To understand the effect of purge strategy on hydrogen consumption for the H-500 DEA-PEMFC, Fig. 5 shows the hydrogen consumption at various purge durations. For this purpose, the PEMFC is tested under a constant purge interval of 8 s as an example, combined with different purge durations (200 ms, 400 ms, 600 ms, and 1000 ms). The main goal of the proposed test is to analyze the impact of wasted hydrogen during purge process on the total hydrogen consumption. It should be noted that during the experiments, the PEMFC voltage remains stable under different purge strategies.

TABLE VI
APPROPRIATE PURGE DURATION FOR EACH PURGE INTERVAL

Purge interval (s)	Appropriate purge duration (ms)
8	200
10	300
12	300
14	400
16	500
18	500
20	600

The duration of each purge strategy test is 100 s, and hydrogen consumption data from the hydrogen flowmeter are recorded during the tests. According to the experimental data, when the purge valve opens, the hydrogen flow shows a peak in the recorded data. This peak represents the wasted hydrogen during the purge process. The total hydrogen consumption is the sum of the hydrogen flow at each current level and the wasted hydrogen during the purge process over the test period. This total is then divided by the test duration to express the result in grams per second. The black stem labeled "Baseline" represents only the hydrogen directly consumed electrochemically by the PEMFC stack to produce power at a given current, without considering the wasted hydrogen used during the purge process. According to Fig. 5, as the purge duration increases, the valve remains open longer, leading to more wasted hydrogen. For a given power with stable voltage, an increase in wasted hydrogen leads to higher total hydrogen consumption and a reduction in PEMFC system efficiency. Therefore, in addition to maintaining voltage stability, selecting a suitable and efficient purge strategy to minimize wasted hydrogen has a significant impact on overall PEMFC system efficiency. As a result, Fig. 5 illustrates that the wasted hydrogen during the purge process should not be neglected, as it significantly contributes to total hydrogen consumption and impacts the system efficiency of the PEMFC.

D. Designing an Efficient Purge Strategy

To efficiently select a suitable purge strategy, two criteria should be considered. The first is voltage stability, and the second is hydrogen consumption. Hydrogen consumption significantly affects energy efficiency and is a major contributor to the PEMFC operating cost. Therefore, an efficient purge strategy involves balancing the trade-off between maintaining voltage stability and minimizing hydrogen consumption. To illustrate this trade-off, this study analyzes the total energy loss (TEL).

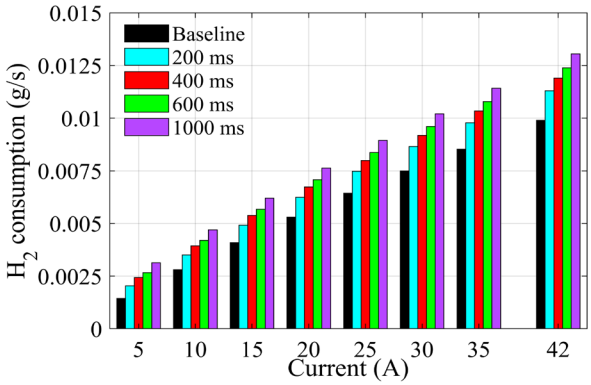

Fig. 5. Impact of wasted hydrogen during the purge process on total hydrogen consumption.

According to (1), the TEL comprises the electrical energy loss (EEL) resulting from the voltage drop and the hydrogen energy loss (HEL) due to the discharged hydrogen.

$$TEL\ (J) = EEL\ + HEL \tag{1}$$

The EEL is calculated as:

$$EEL\ (J) = N \times \int_{0}^{Purge\ period} (V_{desired} - V(t))\ I\ dt \tag{2}$$

where N is the number of purge periods within 100 s test, I represents the PEMFC current, $V_{desired}$ is the PEMFC nominal voltage for a given current, and $V(t)$ is the experimental PEMFC voltage. The HEL can be calculated using (3).

$$HEL\ (J) = N \times discharged\ H_2\ \times LHV \tag{3}$$

In (3), $discharged\ H_2$ represents the amount of wasted hydrogen in grams, and LHV stands for the lower heating value of hydrogen. To better understand the amount of energy loss, this study presents energy loss as a percentage of the total produced energy (TPE). The TPE is defined as:

$$TPE\ (J) = \left(N \times \int_{0}^{Purge\ period} (V(t))I\ dt\right) + TEL \tag{4}$$

Therefore, the ratio of energy loss to TPE is defined as:

$$\begin{aligned} TEL_r\ (\%) &= TEL/TPE \\ EEL_r\ (\%) &= EEL/TPE \\ HEL_r\ (\%) &= HEL/TPE \end{aligned} \tag{5}$$

Fig. 6 shows the ratio of energy loss to TPE as a percentage. Fig. 6 represents the average value for all currents to provide a clear perspective on energy loss. The results from Fig. 6(a) show that longer purge intervals reduce the frequency of purging, which results in lower hydrogen consumption and reduced HEL. However, longer intervals can increase the risk of water management faults and result in voltage drops and an increase in EEL. The results illustrate that up to a 12 s purge interval, the TEL decreases because hydrogen consumption is reduced as the purge interval increases, and the voltage drop is not severe. However, after the 12 s purge interval, although hydrogen consumption continues to decrease, the voltage drop caused by the longer purge interval becomes the dominant factor, leading to an increase in TEL. According to Fig. 6(b), across different purge durations, an increase in purge duration leads to a longer opening time of the purge valve, which results in increased HEL and reduces the risk of water management faults, leading to lower EEL. The results show that up to 500 ms, hydrogen consumption does not have a predominant effect, and the decrease in EEL and the reduced risk of water management faults cause a reduction in TEL. However, after 500 ms, the increase in hydrogen consumption becomes the predominant factor, leading to an increase in TEL. The results indicate that a long purge interval and short purge duration reduce HEL but increase EEL. On the other hand, a short purge interval and long purge duration reduce EEL but increase HEL.

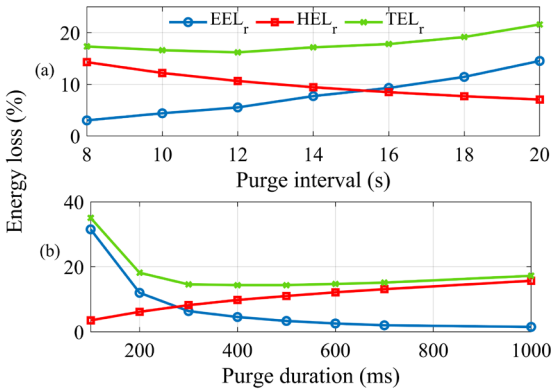

Fig. 6. Ratio of energy loss to TPE based on: (a) Purge interval; (b) Purge duration.

In summary, Fig. 6 illustrates that, in addition to EEL, which is related to voltage stability, HEL, which is related to hydrogen consumption, is equally important. As a result, selecting an efficient purge strategy to reduce TEL involves a trade-off between balancing hydrogen consumption (HEL) and voltage drop (EEL).

1) Adaptive Efficient Purge Strategy Framework: This section aims to design an adaptive efficient purge strategy that adjusts to different current levels. An adaptive efficient purge strategy consists of two steps. In the first step, all combinations of different purge intervals and durations, forming 56 various purge strategies, are analyzed for each current level from 1 A to 42 A. Among these, the combinations with a voltage drop of less than 100 mV are selected. The next step is to examine hydrogen consumption. Among the combinations that maintain voltage stability, the one with the lowest wasted hydrogen is selected as the efficient purge strategy. This procedure is repeated whenever the PEMFC operating current changes.

Fig. 7 illustrates the process of selecting an adaptive efficient purge strategy based on different current levels. It should be noted that the results shown in Fig. 7 are based on data extracted from the extensive experiments described in Section II. According to Fig. 7 the red stems represent combinations where the voltage drop exceeds 100 mV threshold which leads to water management faults. The blue stems represent combinations where the voltage drop stays below 100 mV which prevents water management faults.

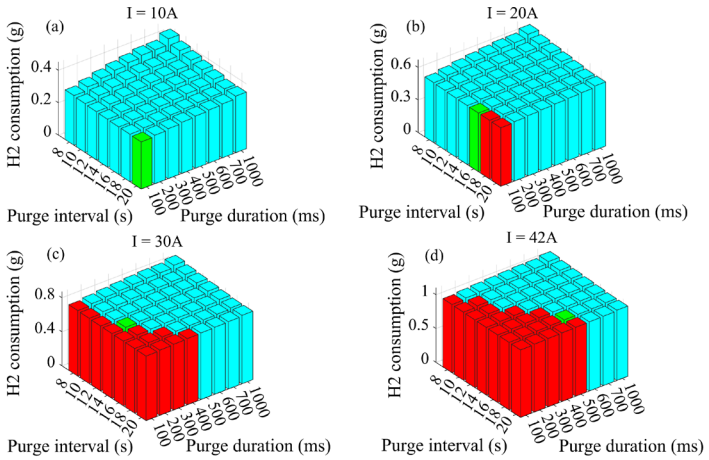

Fig. 7. Adaptive efficient purge strategy selection for different current levels: (a) 10 A; (b) 20 A; (c) 30 A; (d) 42 A.

Among the blue stems, which represent combinations with voltage drops under 100 mV, the one with the lowest wasted hydrogen is chosen as the efficient purge strategy and is marked by the green stem. As a result, the priority of the proposed purge strategy is to maintain voltage stability. The strategy initially selects purge combinations that ensure stable voltage. Then, among these combinations, the one with the minimum wasted hydrogen and lower hydrogen consumption is chosen as the efficient purge strategy. This procedure illustrates that the proposed purge strategy does not compromise voltage stability in order to reduce hydrogen consumption.

To illustrate the effectiveness of the proposed purge strategy, Fig. 8 compares the experimental results of the proposed purge strategy with the non-adaptive purge strategy recommended by the manufacturer. According to Fig. 8(a)-(b), the manufacturer's suggested strategy uses a constant purge period for all current levels. According to Fig. 8(c), the manufacturer's purge strategy works effectively up to 24 A. However, it fails to mitigate water management faults and maintain voltage stability at higher currents. As shown in Fig. 8(c), the proposed purge strategy keeps the voltage drop below 100 mV across different current levels due to its adaptive feature, demonstrating its effectiveness in improving water management.

III. Integrated Water Management into the Energy Management Strategy

A. Hardware-in-the-Loop Setup

To evaluate the effectiveness of the proposed purge strategy for water management in real-time application, this study aims to design an IWM-EMS through a HIL platform for a multi-stack hybrid powertrain case study used for a low-speed vehicle called Nemo [32]. The powertrain includes four H-500 DEA-PEMFCs, a three-phase induction motor, and a battery pack. The FCs serve as the main power source, while the battery pack is small, and its main role is to assist the FCs in supplying power peaks. In this powertrain configuration, the battery pack connects directly to the bus, while the FCs are connected through unidirectional DC-DC converters. The proposed IWM-EMS consists of an EMS level and a purge strategy level.

The proposed IWM-EMS is programmed in MATLAB and embedded into the LabVIEW environment. The time step of the proposed IWM-EMS is one second.

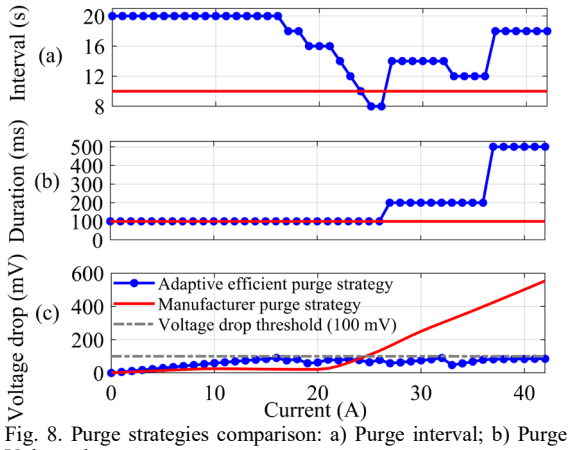

Fig. 8. Purge strategies comparison: a) Purge interval; b) Purge duration; c) Voltage drop.

In each time step, the IWM-EMS determines the optimal power of each sub-stack through the EMS level and the efficient purge strategy based on the reference current through the purge strategy level. After receiving the reference current and determining the efficient purge interval and duration, the control signal for the purge valve is sent to the PEMFC controller through the LabVIEW interface block.

The HIL platform is shown in Fig. 9. According to Fig. 9, two H-500 DEA-PEMFCs in this platform are employed as real components, while the other two PEMFCs are virtual and used as emulators. It should be mentioned that the other components of this platform are represented by mathematical models. The PEMFCs are connected to a National Instruments CompactRIO (NIcRIO-9022) through their controller. The CompactRIO connects to the PC running LabVIEW software using an Ethernet connection. Data is transferred between the CompactRIO and the PC every 100 ms. It should be mentioned that the time scale of flooding and drying out dynamics ranges from a few seconds to several minutes [33]. Therefore, the order of magnitude of the sampling rate (100 ms) is much faster than the characteristic time of flooding and drying out dynamics. In this regard, 100 ms is considered a conservative sampling rate to ensure a fast response to voltage changes caused by water management faults. At each sampling time, experimental data such as PEMFC voltage, current, and hydrogen flow rate are recorded and collected. Two 8514 BK Precision DC electronic loads are used to impose load profiles on the PEMFC stacks.

The model of the two PEMFC emulators is based on the Amphlett model, which is a semi-empirical model supported by a mechanistic background and has been widely used in many studies due to its strong capacity to model PEMFC output voltage [34]. The nominal output voltage of the PEMFC is calculated using (6).

$$V_{nominal} = N_{cell}(E_{Nernst} + V_{act} + V_{ohm} + V_{con}) \tag{6}$$

where N_{cell} is the number of cells, E_{Nernst} (V) is reversible potential, V_{act} (V), V_{ohm} (V), and V_{con} (V) are the activation loss, ohmic loss, and concentration loss, respectively. E_{Nernst} is calculated using (7):

$$E_{Nernst} = 1.299 - 0.85 \times 10^{-3}(T_{st} - 298.15) + 4.3085 \times 10^{-5}[0.5ln(P_{O2} + ln(P_{H2})]\, T_{st} \tag{7}$$

where T_{st} is the stack temperature (K), P_{O2} and P_{H2} are the oxygen and hydrogen partial pressures (N/m²). The formulation of V_{act} is shown in (8).

$$V_{act} = -[\xi_1 + \xi_2 T_{st} + \xi_3 T_{st} ln(CO_2) + \xi_4 T_{st} ln(i_{FC})] \tag{8}$$

where ξ_n (n = 1...4) are semi-empirical parameters, CO_2 is the oxygen concentration (mol/cm³), and i_{FC} is the PEMFC current (A). V_{ohm} and V_{con} can be calculated by:

$$V_{ohmic} = -i_{FC} R_{int} = -i_{FC}(\zeta_1 + \zeta_2 T_{st} + \zeta_3 i_{FC}) \tag{9}$$

$$V_{con} = B \times ln(1 - \frac{J}{J_{max}}) \tag{10}$$

where R_{int} (Ω) is the PEMFC equivalent internal resistance, ζ_n (n = 1...3) and B are semi-empirical coefficients, J is the actual current density (A/cm²), and J_{max} is the maximum current density (A/cm²).

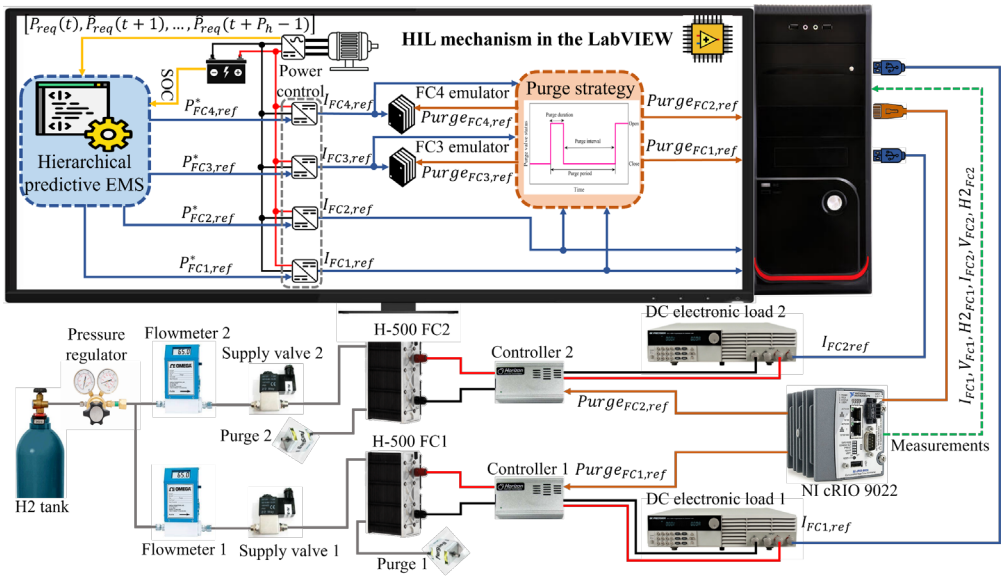

Fig. 9. HIL mechanism of the IWM-EMS.

Based on the data extracted from the extensive experiments, the voltage drop corresponding to different purge strategies for each current level is calculated and collected in a lookup table. In this regard, the PEMFC output voltage at each time step is calculated using (11).

$$V_{FC} = V_{nominal} - V_{drop} \tag{11}$$

where V_{drop} is the PEMFC voltage drop during the purge interval. The voltage drop is subtracted from the PEMFC output voltage model to make the model more realistic.

In the HIL setup, a PI controller is designed in the power control box to regulate the PEMFC current and ensure accurate tracking of the reference power. In this setup, when V_{FC} decreases due to a voltage drop, the PI controller increases the PEMFC operating current to reach the reference power.

B. Energy Management Strategy Level

In this study, a hierarchical predictive EMS (HPEMS) is used to distribute optimal power. The first layer is a RB strategy that decides how many FCs should be activated and participate in the second layer. The second layer is a model predictive control (MPC) that, based on the information from the first layer and system constraints, determines optimal power between the FCs and the battery.

Upper Layer

The upper layer is a RB-EMS that uses a rotary state machine approach to determine how many sub-stacks should participate in the lower layer. This decision is made based on the requested power, battery SOC, and sub-stack degradation rate. In other words, at each time step, sub-stacks with lower degradation rates are given higher priority to participate in the lower layer of the EMS. For example, if two sub-stacks are sufficient to meet the requested power, the upper layer selects the two sub-stacks with the lowest degradation. As a result, the upper layer of the EMS serves two main purposes. First, it aims to balance degradation across all sub-stacks and prevent further degradation. Second, it helps reduce hydrogen consumption by determining when to activate or deactivate sub-stacks, keeping unnecessary FCs turned off when not required.

Lower Layer

The lower layer of the EMS employs MPC, a predictive OB strategy. Based on the future vehicle velocities within a prediction horizon of 10 s and utilizing information from the upper layer regarding the number of active sub-stacks, the MPC minimizes a cost function to determine the optimal power distribution between the sub-stacks and the battery. In other words, at each time step, the lower layer determines the optimal power for each sub-stack, and the reference current corresponding to the optimal power is sent to the purge strategy level. The nonlinear problem is formulated as a state-space model in MPC. Usually, in this type of problem, the SOC is a state variable, and FC power is the control variable. In this study, the increment of FC power is used as the control variable, with the state-space formulation given by (12).

$$\Delta x(t+1) = A\Delta x(t) + B\Delta u(t) + D\Delta d(t) \tag{12}$$

where $x(t)$ represents the SOC, $u(t)$ is the FC power, and $d(t)$ is the requested power, modeled as a disturbance in this formulation. A, B, and D are matrices of coefficients and t indicates the time step. In this study the sampling time is set to 1 s. It should be noted that in this paper, prediction horizon (P_h) is set to 10 s. The MPC requires the vehicle's future velocities within the prediction horizon to determine the optimal power sequence. For this purpose, this study assumes that the entire driving cycle is already known, and at each time step, using the next 10 s of velocity data, the MPC determines the optimal power sequence. As shown in (13), the multi-objective cost function in this study is based on the total operating cost, which includes hydrogen consumption, FC degradation, and battery degradation.

$$\min_{\Delta P_{FC}(t+k),k\in\{0,1,\dots,P_h-1\}} J_t = C_{H_2,t} + C_{FC,deg,t} + C_{bat,deg,t} + k_{SOC,t} \ (\$) \tag{13}$$

where $C_{H_2,t}$ is the hydrogen consumption cost, $C_{FC,deg,t}$ is the FC degradation cost. and $C_{bat,deg,t}$ is the battery degradation cost. The final term in the multi-objective cost function, $k_{SOC,t}$, is a penalty term designed to enforce the battery charge-sustaining strategy and keep the SOC close to its initial value. In this study, the units for hydrogen price, FC system price, and battery pack price are 4 $/kg, 93 $/kW, and 178.41 $/kWh, respectively [35], [36]. FC operation constraints are shown in (14).

$$\begin{cases} P_{FC,min} \le P_{FC}(t+k) \le P_{FC,max} \\ \Delta P_{FC,min} \le P_{FC}(t+k) - P_{FC}(t+k-1) \le \Delta P_{FC,max} \end{cases} \tag{14}$$

$P_{FC,min}$ is set to zero, $P_{FC,max}$ is 500 W, and $\Delta P_{FC,min}$ and $\Delta P_{FC,max}$ are -50 W/s and 50 W/s, respectively. Battery constraints include battery power, SOC, and SOH, as shown in (15).

$$\begin{cases} SOC(0) = 70\% \\ SOC_{min} \le SOC(t+k) \le SOC_{max} \\ SOH(0) = 100\% \\ SOH_{min} \le SOH(t+k) \le SOH_{max} \\ P_{bat,min} \le P_{bat}(t+k) \le P_{bat,max} \end{cases} \tag{15}$$

where SOC_{min} is 50%, SOC_{max} is 90%, SOH_{min} is 0%, and SOH_{max} is 100%. The battery power limits, $P_{bat,min}$ and $P_{bat,max}$, are set to -1900 W and 1900 W, respectively. This study utilizes sequential quadratic programming (SQP) to solve the receding horizon optimization problem, which is a common algorithm for such applications. The convergence and computational efficiency of SQP are satisfactory for use in real-time applications [36], [37].

C. Purge Strategy Level

The second level of the proposed AIWM-EMS is the purge strategy section. This level uses an adaptive efficient purge strategy mechanism. The proposed purge strategy is based on a lookup table extracted from extensive experiments. At each time step, the purge strategy block receives the reference current from the EMS, determines the efficient purge strategy that maintains stable voltage and minimizes wasted hydrogen, and then sends the control signal to the purge valve through the PEMFC controller. It should be noted that, at each time step, the purge strategy level receives four different current values corresponding to the four sub-stacks. Based on the reference current of each sub-stack, it determines the efficient purge interval and duration.

IV. Result and Discussion

This section aims to evaluate the IWM-EMS performance. This study proposes an adaptive IWM-EMS (AIWM-EMS), where an adaptive efficient purge strategy is integrated into the EMS. The performance of the AIWM-EMS is compared with that of the non-adaptive IWM-EMS (NAIWM-EMS), which incorporates the manufacturer's non-adaptive purge strategy into the EMS. The performance and effectiveness of the two IWM-EMSs are compared under the WLTC-class3 driving cycle. Fig. 10 shows the driving cycle, with the right vertical axis representing the requested power and the left vertical axis representing the velocity.

Fig. 11(a)-(d) show the FC power distribution, and Fig. 11(e) presents the battery SOC. FC1 and FC2 are real PEMFCs in the HIL, with experimental data such as current, voltage, and hydrogen consumption collected via CompactRIO, while FC3 and FC4 are emulators. According to Fig. 11(a)-(d), in high-power zones, such as from 1113 s to 1372 s and 1546 s to 1770 s, the FCs must operate at high currents to meet the requested power. FCs operating under the AIWM-EMS can supply the requested power because water management faults are effectively mitigated and the FCs voltage remains stable. To meet the requested power, FCs under the NAIWM-EMS must operate at higher currents than those under the AIWM-EMS to compensate for the higher voltage drop. FCs under the NAIWM-EMS operate at lower power at the maximum FC current. With the maximum current set to 42 A, the FCs under NAIWM-EMS cannot exceed this current to compensate for the voltage drop and must operate at reduced power. Operating at reduced power causes FCs in the NAIWM-EMS to work longer in the high-power zone compared to those in the AIWM-EMS to meet the requested power and maintain battery SOC, resulting in a different SOC trajectory, as shown in Fig. 11(e).

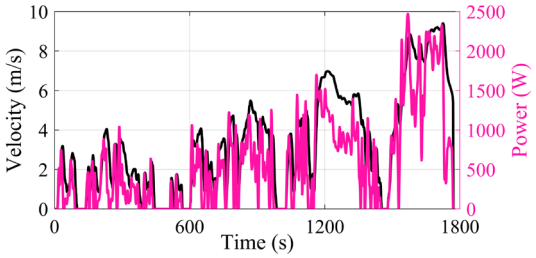

Fig. 10. WLTC-class3 driving cycle.

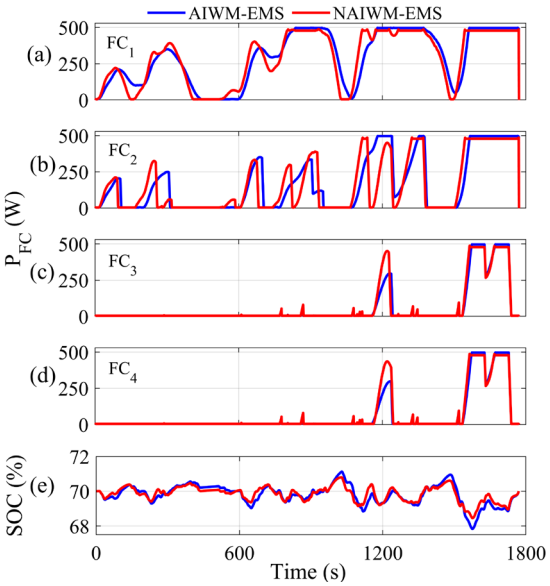

Fig. 11. AIWM-EMS and NAIWM-EMS performance under the WLTC-class3 driving cycle: a) FC_1 power; b) FC_2 power; c) FC_3 power; d) FC_4 power; e) Battery SOC.

Fig. 12 illustrates the voltage drop caused by water management faults in the PEMFCs during the driving cycle. The ultimate goal of a suitable purge strategy is to improve water management, reduce voltage drops, and enhance PEMFC voltage stability. The results of the HIL show that the AIWM-EMS consistently maintains voltage stability throughout the driving cycle, keeping voltage drops below 100 mV. This demonstrates the effectiveness of the proposed strategy in mitigating water management faults. These results highlight the robustness and quick response time of the adaptive strategy under real driving conditions. However, the voltage drop of the FCs under the NAIWM-EMS exceeds 100 mV, particularly in high-power zones, indicating water flooding faults due to the use of a non-adaptive purge strategy.

Fig. 13 shows a comparison of the total wasted hydrogen when the purge valve is open. During the driving cycle, opening the PEMFC purge valve causes a peak in the hydrogen flow data, which indicates the amount of wasted hydrogen during the purge process. Over the entire driving cycle, all hydrogen flow peaks are extracted and calculated as the total wasted hydrogen under two different purge strategies. The total wasted hydrogen in the AIWM-EMS is 1.128 g, while it is 1.533 g in the NAIWM-EMS. According to Fig. 13, the total wasted hydrogen in the AIWM-EMS is 26.42% less than in the NAIWM-EMS.

Fig. 14 compares the total operating cost of the FC-HEV under the AIWM-EMS and NAIWM-EMS. According to Fig. 14, the cost of hydrogen consumption in the AIWM-EMS is 4.09% lower than in the NAIWM-EMS.

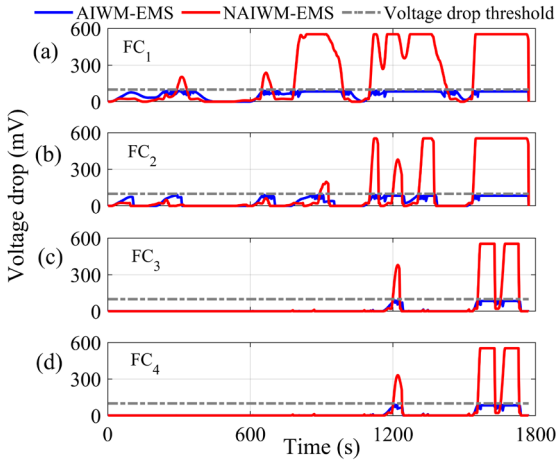

Fig. 12. Voltage drop comparison between AIWM-EMS and NAIWM-EMS: a) FC_1; b) FC_2; c) FC_3; d) FC_4.

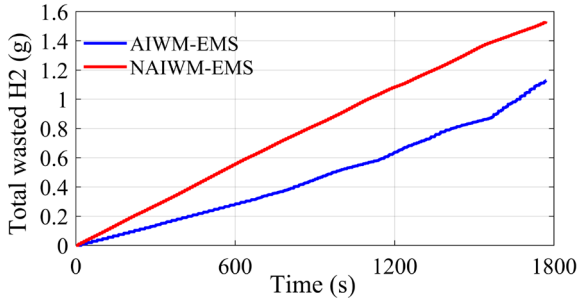

Fig. 13. Total wasted hydrogen during the purge strategies.

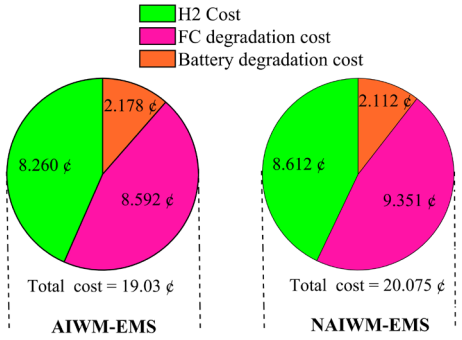

Fig. 14. FC-HEV operating cost comparison.

The results also show that the cost of FC degradation in the AIWM-EMS is 8.12% less than in the NAIWM-EMS. Under the NAIWM-EMS, the FCs operate at reduced power at maximum current, leading to longer operation at high power to meet the requested power and maintain battery SOC, which increases FC degradation. The results indicate that the total time spent in high power for all FCs in the AIWM-EMS is 1189 s, while in the NAIWM-EMS, the FCs spend 1263 s in the high-power zone. The cost of battery degradation in the AIWM-EMS is slightly higher than in the NAIWM-EMS because the AIWM-EMS utilizes a wider range of battery SOC. The results show that the total operating cost in the AIWM-EMS is 5.21% lower than in the NAIWM-EMS. As a result, according to the HIL results, the proposed strategy, due to its adaptability, can dynamically adjust to changes in the requested power. Compared to the constant and non-adaptive strategy, the ability of the proposed strategy to adapt to various dynamic conditions leads to improved voltage stability, lower hydrogen consumption, reduced FC degradation, and ultimately a lower operating cost. On the other hand, reducing the total operating cost of the FC has a direct impact on maintenance cost. Increased voltage stability and reduced FC degradation lead to a longer FC lifespan, which delays maintenance, reduces its frequency, and ultimately lowers maintenance cost.

Fig. 15 shows the system efficiency distribution of all sub-satcks in the FC-HEV. According to (16), the FC system efficiency is calculated as follows:

$$\eta_{FC\ system} = \frac{P_{FC,total}}{\dot{m}_{H_2,total}\, LHV_{H_2}} \tag{16}$$

where $P_{FC,total}$ is the total power output of the four sub-stacks, $\dot{m}_{H_2,total}$ is the total hydrogen consumption by the four sub-stacks, and LHV_{H_2} is the lower heating value of hydrogen, which is 120 MJ/kg.

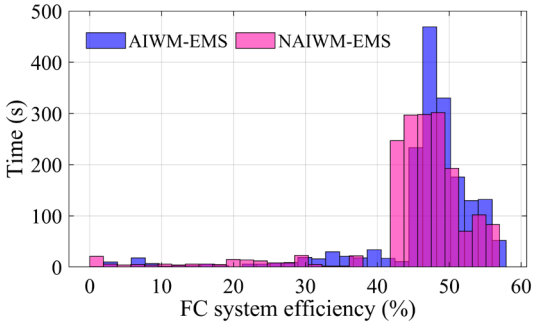

Fig. 15. FC system efficiency distribution comparison.

At each time step of the driving cycle, the FC system efficiency is calculated and recorded. To evaluate the impact of the AIWM-EMS on multi-stack FC performance, this study analyzes the multi-stack FC system efficiency over the entire driving cycle tested in the HIL. In this regard, according to the experimental results, the maximum system efficiency of the tested PEMFC is 46.5%, and the high-efficiency zone is defined as the region where the PEMFC system efficiency is equal to or greater than 45%. The high-efficiency zone is the area where the PEMFC achieves high performance and lower hydrogen consumption per unit of power output. In the AIWM-EMS, the FCs operate in a safe condition without water management faults, resulting in voltage drops below 100 mV. This prevents the FCs from operating at higher currents and increasing hydrogen consumption, thereby achieving higher efficiency, as shown in Fig. 15. Additionally, in the AIWM-EMS, the efficient purge strategy minimizes wasted hydrogen. Consequently, the FCs operates with higher efficiency compared to the NAIWM-EMS. However, it should be mentioned that increasing efficiency and reducing hydrogen consumption do not mean that the proposed strategy compromises voltage stability. The strategy first ensures voltage stability, and among the suitable purge strategies that maintain voltage stability, it selects the efficient one with minimum wasted hydrogen.

The results show that the FCs operate 78.36% of the driving cycle time in a high-efficiency zone, while in the NAIWM-EMS, the FCs operate 62% of the driving cycle time in the high-efficiency zone.

V. Conclusion

This study aims to integrate the impact of water management into the EMS for a FC-HEV. For this purpose, an IWM-EMS is designed with two levels. The first level is the HPEMS and the second level is the purge strategy. This paper proposes an AIWM-EMS in which an adaptive efficient purge strategy is embedded. The AIWM-EMS adapts to various dynamic conditions by adjusting the purge strategy based on the PEMFC operating current levels. On the other hand, the AIWM-EMS selects the efficient purge strategy to mitigate water management faults, enhance voltage stability, and minimize hydrogen consumption. The results of the AIWM-EMS are compared with the NAIWM-EMS, which includes a non-adaptive purge strategy recommended by the FC manufacturer. The results demonstrate the effectiveness of the AIWM-EMS in reducing water management faults, maintaining voltage stability across all current levels, and minimizing hydrogen consumption. The costs of hydrogen consumption and FC degradation in the FC-HEV under the AIWM-EMS are 4.09% and 8.12% lower, respectively, than in the NAIWM-EMS, and the total operating cost in the AIWM-EMS is reduced by 5.21% compared to the NAIWM-EMS. The results also show that the FCs under the AIWM-EMS works 78.36% of the operating time in the high-efficiency zone, compared to 62% under the NAIWM-EMS.

Future Work

1- To develop the proposed purge strategy and increase its effectiveness, a feasible option for future work is to expand the experiments and evaluate the strategy by considering changes in environmental conditions such as temperature and humidity.

2- Integrating a FC maintenance cost model into the total operating cost in future work will help account for all real-world FC expenses and enhance the practicality of the proposed purge strategy in real-world applications.

3- This study aimed to illustrate the importance of water management in PEMFC performance and operating cost. Thermal management and operating temperature can significantly affect water management and overall PEMFC performance. Therefore, in future work, the authors plan to enhance the performance and applicability of the proposed purge strategy by incorporating the effects of different cooling systems and thermal management into the water management approach.

References

[1] M. S. Munsi and R. P. Joshi, “Comprehensive Analysis of Fuel Cell Electric Vehicles: Challenges, Powertrain Configurations, and Energy Management Systems,” *IEEE Access*, vol. 12, no. September, pp. 145459–145482, 2024, doi: 10.1109/ACCESS.2024.3472704.

[2] X. Hu, J. Han, X. Tang, and X. Lin, “Powertrain Design and Control in Electrified Vehicles: A Critical Review,” *IEEE Trans. Transp. Electrif.*, vol. 7, no. 3, pp. 1990–2009, 2021, doi: 10.1109/TTE.2021.3056432.

[3] A. Prasanthi, H. Shareef, R. Errouissi, G. V. Murugesu, and M. Asna, “Optimal Sizing and Dynamic Energy Source Characteristics of Hybrid Electric Vehicles: A Comprehensive Review and Future Directions,” *IEEE Access*, vol. 12, no. March, pp. 44695–44729, 2024, doi: 10.1109/ACCESS.2024.3380464.

[4] A. Khalatbarisoltani, H. Zhou, X. Tang, M. Kandidayeni, L. Boulon, and X. Hu, “Energy Management Strategies for Fuel Cell Vehicles: A Comprehensive Review of the Latest Progress in Modeling, Strategies, and Future Prospects,” *IEEE Trans. Intell. Transp. Syst.*, vol. 25, no. 1, pp. 14–32, 2024, doi: 10.1109/TITS.2023.3309052.

[5] A. Moslehi, M. Kandidayeni, M. Hébert, and S. Kelouwani, “Investigating the impact of a fuel cell system air supply control on the performance of an energy management strategy,” *Energy Convers. Manag.*, vol. 325, p. 119374, 2025, doi: https://doi.org/10.1016/j.enconman.2024.119374.

[6] M. S. Munsi and H. Chaoui, “Energy Management Systems for Electric Vehicles: A Comprehensive Review of Technologies and Trends,” *IEEE Access*, vol. 12, no. December 2023, pp. 60385–60403, 2024, doi: 10.1109/ACCESS.2024.3371483.

[7] F. Tao, L. Zhu, Z. Fu, P. Si, and L. Sun, “Frequency decoupling-based energy management strategy for fuel cell/ battery/ultracapacitor hybrid vehicle using fuzzy control method,” *IEEE Access*, vol. 8, pp. 166491–166502, 2020, doi: 10.1109/ACCESS.2020.3023470.

[8] A. M. I. Fernandez *et al.*, “An Adaptive State Machine Based Energy Management Strategy for a Multi-Stack Fuel Cell Hybrid Electric Vehicle,” *IEEE Trans. Veh. Technol.*, vol. 69, no. 1, pp. 220–234, 2020, doi: 10.1109/TVT.2019.2950558.

[9] D. F. Pereira, F. D. C. D. C. Lopes, and E. H. Watanabe, “Nonlinear Model Predictive Control for the Energy Management of Fuel Cell Hybrid Electric Vehicles in Real Time,” *IEEE Trans. Ind. Electron.*, vol. 68, no. 4, pp. 3213–3223, 2021, doi: 10.1109/TIE.2020.2979528.

[10] Y. Zhang, R. Ma, D. Zhao, Y. Huangfu, and W. Liu, “An Online Efficiency Optimized Energy Management Strategy for Fuel Cell Hybrid Electric Vehicles,” *IEEE Trans. Transp. Electrif.*, vol. 9, no. 2, pp. 3203–3217, 2023, doi: 10.1109/TTE.2022.3214683.

[11] Z. Fu, H. Wang, F. Tao, B. Ji, Y. Dong, and S. Song, “Energy Management Strategy for Fuel Cell/Battery/Ultracapacitor Hybrid Electric Vehicles Using Deep Reinforcement Learning With Action Trimming,” *IEEE Trans. Veh. Technol.*, vol. 71, no. 7, pp. 7171–7185, 2022, doi: 10.1109/TVT.2022.3168870.

[12] Y. Zhang, R. Ma, D. Zhao, Y. Huangfu, and W. Liu, “A Novel Energy Management Strategy Based on Dual Reward Function Q-Learning for Fuel Cell Hybrid Electric Vehicle,” *IEEE Trans. Ind. Electron.*, vol. 69, no. 2, pp. 1537–1547, 2022, doi: 10.1109/TIE.2021.3062273.

[13] R. Ma, H. Dang, R. Xie, L. Xu, and D. Zhao, “Online Fault Diagnosis for Open-Cathode PEMFC Systems Based on Output Voltage Measurements and Data-Driven Method,” *IEEE Trans. Transp.*

Electrif., vol. 8, no. 2, pp. 2050–2061, 2022, doi: 10.1109/TTE.2021.3114194.
[14] G. Dotelli, R. Ferrero, P. G. Stampino, S. Latorrata, and S. Toscani, "PEM Fuel Cell Drying and Flooding Diagnosis With Signals Injected by a Power Converter," *IEEE Trans. Instrum. Meas.*, vol. 64, no. 8, pp. 2064–2071, 2015, doi: 10.1109/TIM.2015.2406051.
[15] S. G. Kandlikar, M. L. Garofalo, and Z. Lu, "Water management in a PEMFC: Water transport mechanism and material degradation in gas diffusion layers," *Fuel Cells*, vol. 11, no. 6, pp. 814–823, 2011, doi: 10.1002/fuce.201000172.
[16] J. Liu, Q. Li, H. Yang, Y. Han, S. Jiang, and W. Chen, "Sequence Fault Diagnosis for PEMFC Water Management Subsystem Using Deep Learning with t-SNE," *IEEE Access*, vol. 7, pp. 92009–92019, 2019, doi: 10.1109/ACCESS.2019.2927092.
[17] A. Alyakhni, L. Boulon, J. M. Vinassa, and O. Briat, "A Comprehensive Review on Energy Management Strategies for Electric Vehicles Considering Degradation Using Aging Models," *IEEE Access*, vol. 9, pp. 143922–143940, 2021, doi: 10.1109/ACCESS.2021.3120563.
[18] Z. Zhang *et al.*, "Research on shutdown purge characteristics of proton exchange membrane fuel cells: Purge parameters conspicuity and residual water," *Appl. Therm. Eng.*, vol. 249, no. May, p. 123437, 2024, doi: 10.1016/j.applthermaleng.2024.123437.
[19] G. Yang, K. Meng, Q. Deng, W. Chen, and B. Chen, "Numerical investigation and experimental verification of liquid water dynamic transfer characteristics in the flow field of PEMFC with dead-ended anode during gas purging," *Chem. Eng. J.*, vol. 491, no. December 2023, p. 152082, 2024, doi: 10.1016/j.cej.2024.152082.
[20] L. shi, P. Liu, M. Zheng, and S. Xu, "Numerical study on the mechanism of water and gas phase transition and water redistribution after purging based on two-dimensional multi-phase model," *Energy Convers. Manag.*, vol. 278, no. January, p. 116725, 2023, doi: 10.1016/j.enconman.2023.116725.
[21] T. Donateo, "Simulation Approaches and Validation Issues for Open-Cathode Fuel Cell Systems in Manned and Unmanned Aerial Vehicles," *Energies*, vol. 17, no. 4, 2024, doi: 10.3390/en17040900.
[22] T. Niu *et al.*, "Purge strategy analysis of proton exchange membrane fuel cells based on experiments and comprehensive evaluation method," *Fuel*, vol. 363, no. November 2023, p. 130970, 2024, doi: 10.1016/j.fuel.2024.130970.
[23] S. Liu *et al.*, "Study on the effect of purging time on the performance of PEMFC with dead-ended anode under gravity," *Renew. Energy*, vol. 200, no. October, pp. 1141–1151, 2022, doi: 10.1016/j.renene.2022.10.065.
[24] J. Shen, Z. Tu, and S. H. Chan, "Effect of gas purging on the performance of a proton exchange membrane fuel cell with dead-ended anode and cathode," *Int. J. Energy Res.*, vol. 45, no. 10, pp. 14813–14823, 2021, doi: 10.1002/er.6757.
[25] J. Yao *et al.*, "High-stability dead-end anode proton exchange membrane fuel cells by purge optimization," *J. Power Sources*, vol. 595, no. December 2023, 2024, doi: 10.1016/j.jpowsour.2024.234062.
[26] J. C. Kurnia, A. P. Sasmito, and T. Shamim, "Advances in proton exchange membrane fuel cell with dead-end anode operation: A review," *Appl. Energy*, vol. 252, no. November 2018, p. 113416, 2019, doi: 10.1016/j.apenergy.2019.113416.
[27] Q. Jian, L. Luo, B. Huang, J. Zhao, S. Cao, and Z. Huang, "Experimental study on the purge process of a proton exchange membrane fuel cell stack with a dead-end anode," *Appl. Therm. Eng.*, vol. 142, no. March, pp. 203–214, 2018, doi: 10.1016/j.applthermaleng.2018.07.001.
[28] Y. F. Lin and Y. S. Chen, "Experimental study on the optimal purge duration of a proton exchange membrane fuel cell with a dead-ended anode," *J. Power Sources*, vol. 340, pp. 176–182, 2017, doi: 10.1016/j.jpowsour.2016.11.039.
[29] I. Dashti, S. Asghari, M. Goudarzi, Q. Meyer, A. Mehrabani-Zeinabad, and D. J. L. Brett, "Optimization of the performance, operation conditions and purge rate for a dead-ended anode proton exchange membrane fuel cell using an analytical model," *Energy*, vol. 179, pp. 173–185, 2019, doi: 10.1016/j.energy.2019.04.118.
[30] J. Hong, J. Yang, Z. Weng, F. Ma, F. Liang, and C. Zhang, "Review on proton exchange membrane fuel cells: Safety analysis and fault diagnosis," *J. Power Sources*, vol. 617, no. June, p. 235118, 2024, doi: 10.1016/j.jpowsour.2024.235118.
[31] M. Kandidayeni *et al.*, "Efficiency Upgrade of Hybrid Fuel Cell Vehicles' Energy Management Strategies by Online Systemic Management of Fuel Cell," *IEEE Trans. Ind. Electron.*, vol. 0046, no. 6, pp. 1–1, 2021, doi: 10.1109/tie.2020.2992950.
[32] M. Kandidayeni *et al.*, "An Online Energy Management Strategy for a Fuel Cell/Battery Vehicle Considering the Driving Pattern and Performance Drift Impacts," *IEEE Trans. Veh. Technol.*, vol. 68, no. 12, pp. 11427–11438, 2019, doi: 10.1109/TVT.2019.2936713.
[33] E. Dijoux, N. Y. Steiner, M. Benne, M. C. Péra, and B. G. Pérez, "A review of fault tolerant control strategies applied to proton exchange membrane fuel cell systems," *J. Power Sources*, vol. 359, pp. 119–133, 2017, doi: 10.1016/j.jpowsour.2017.05.058.
[34] R. F. Mann, J. C. Amphlett, M. A. I. Hooper, H. M. Jensen, B. A. Peppley, and P. R. Roberge, "Development and application of a generalized steady-state electrochemical model for a PEM fuel cell," *J. Power Sources*, vol. 86, no. 1, pp. 173–180, 2000, doi: 10.1016/S0378-7753(99)00484-X.
[35] M. Moghadari, M. Kandidayeni, L. Boulon, and H. Chaoui, "Predictive Health-Conscious Energy Management Strategy of a Hybrid Multi-Stack Fuel Cell Vehicle," *IEEE Trans. Veh. Technol.*, vol. PP, pp. 1–16, 2024, doi: 10.1109/TVT.2024.3512204.
[36] X. Hu, C. Zou, X. Tang, T. Liu, and L. Hu, "Cost-optimal energy management of hybrid electric vehicles using fuel cell/battery health-aware predictive control," *IEEE Trans. Power Electron.*, vol. 35, no. 1, pp. 382–392, 2020, doi: 10.1109/TPEL.2019.2915675.
[37] A. Khalatbarisoltani, M. Kandidayeni, L. Boulon, and X. Hu, "Power Allocation Strategy based on Decentralized Convex Optimization in Modular Fuel Cell Systems for Vehicular Applications," *IEEE Trans. Veh. Technol.*, vol. 9545, no. c, pp. 14563–14574, 2020, doi: 10.1109/tvt.2020.3028089.

Mohammadreza Moghadari was born in Babol, Iran, in 1992. He received his B.S. in Mechanical Engineering from Islamic Azad University, Tehran, in 2015, and his M.S. (Hons.) in Automotive Engineering from Iran University of Science and Technology in 2018. He began his Ph.D. in 2020 at the Hydrogen Research Institute, Université du Québec à Trois-Rivières (UQTR), Canada. Since 2016, he has published numerous articles in leading SCI journals and served as a reviewer for academic journals. His research focuses on PEMFC systems management, energy management strategies, optimization-based control, and fault-tolerant strategies for hybrid vehicles.

Mohsen Kandidayeni (Member, IEEE) was born in Tehran, Iran, in 1989. He received his B.S. in mechanical engineering in 2011, an M.S. (Hons.) in mechatronics from Arak University, Iran, in 2014, and a Ph.D. (Hons.) in electrical engineering from the University of Quebec at Trois-Rivières (UQTR), Canada, in 2020. From 2020 to 2024, he served as a Postdoctoral Fellow at eTESC, Research Associate and Technical Project Manager at HRI, and is now an Assistant Professor at UQTR. He has authored over 75 journal and conference publications and actively reviews scholarly articles. His research interests include hybrid electric vehicles, fuel cell systems, energy management, multiphysics systems, modeling, and control. Recognized with awards like the FRQNT Doctoral and Postdoctoral Scholarship, Best PhD Thesis Award, and Third Prize in the Energy Research Challenge, he has made significant contributions to energy-related research.

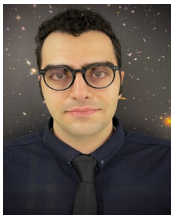

Ashkan Makhsoos was born in Arak, Iran, in 1991. He holds an M.Sc. in Mechanical Engineering of Biosystems (Renewable Energies) from the University of Tehran (2017) and a B.Sc. from the University of Arak (2014), focusing on renewable energies and biofuels. He is a Ph.D. candidate in Electrical Engineering at the University of Quebec at Trois-Rivières, specializing in energy management of multi-stack Proton Exchange Membrane Water Electrolyzers (PEMWE) for hydrogen production from renewable energies. A member of the Institute for Hydrogen

Research (IHR), he contributes to green hydrogen projects and reviews for prestigious journals. His research interests include energy management, electrochemical modeling, and renewable energy systems.

Loïc Boulon (Senior Member, IEEE) received his Master's degree in Electrical and Automatic Control Engineering from the University of Lille, France, in 2006, and a Ph.D. in Electrical Engineering from the University of Franche-Comté, France. He has been a professor at Université du Québec à Trois-Rivières (UQTR) since 2010, becoming a Full Professor in 2016 and Deputy Director of the Hydrogen Research Institute in 2019. His research focuses on modeling, control, and energy management of multiphysics systems, including hybrid electric vehicles and energy sources like fuel cells, batteries, and ultracapacitors. Dr. Boulon has authored over 140 peer-reviewed publications and delivered more than 40 invited talks globally. In 2022, he was recognized among the top researchers in "Proton Exchange Membrane Fuel Cell (PEMFC)" and "Plug-in Hybrid Vehicles" by Elsevier SciVal. He is VP-Motor Vehicles for the IEEE Vehicular Technology Society, holds the Canada Research Chair in Energy Sources for Future Vehicles, and directs the Réseau Québécois sur l'Énergie Intelligente.

Hicham Chaoui (Senior Member, IEEE) received his Ph.D. in Electrical Engineering (with honors) from the University of Quebec, Trois-Rivières, Canada, in 2011. His career spans academia and industry, specializing in control and energy systems. From 2007 to 2014, he held engineering and management roles in the Canadian industry. Currently, he is a Faculty Member at Carleton University, Ottawa, Canada. Dr. Chaoui has authored over 200 journal and conference publications and is a registered Professional Engineer in Ontario. He serves as an Associate Editor for IEEE Transactions on Power Electronics, IEEE Transactions on Vehicular Technology, and other journals. His accolades include the Best Thesis Award, Governor General of Canada Gold Medal, FED Research Excellence Award, Early Researcher Award from the Government of Ontario, and Top Editor Recognition from IEEE Vehicular Technology Society and IEEE Power Electronics Society.